Surface acoustic wave driven ferromagnetic resonance in (Ga,Mn)(As,P) epilayers

L. Thevenard[1,2], C. Gourdon[1,2], J. Y. Prieur[1,2], H. J. von Bardeleben[1,2], S. Vincent[1,2], L. Becerra[1,2], L. Largeau[3], and J.-Y. Duquesne[1,2]

[1] *CNRS, UMR7588, Institut des Nanosciences de Paris, 4 place Jussieu,75252 Paris, France*

[2] *Sorbonne Universités, UPMC Univ Paris 06, UMR7588 4 place Jussieu,75252 Paris, France*

[3] *Laboratoire de Photonique et Nanostructures, CNRS, UPR 20, Route de Nozay, Marcoussis, 91460, France*

(Dated: June 26, 2014)

Interdigitated transducers were used to generate and detect surface acoustic waves on a thin layer of (Ga,Mn)(As,P). The out-of-plane uniaxial magnetic anisotropy of this dilute magnetic semiconductor is very sensitive to the strain of the layer, making it an ideal test material for the dynamic control of magnetization via magneto-striction. The time-domain measurement of the amplitude and phase of the transmitted SAW during magnetic field sweeps indicated a clear resonant behavior at a field close to the one calculated to give a precession frequency equal to the SAW frequency. A resonance was observed from 5K to 85K, just below the Curie temperature of the layer. A full analytical treatment of the coupled magnetization/acoustic dynamics showed that the magneto-strictive coupling modifies the elastic constants of the material and accordingly the wave-vector solution to the elastic wave equation. The shape and position of the resonance were well reproduced by the calculations, in particular the fact that velocity (phase) variations resonated at lower fields than the acoustic attenuation variations.

PACS numbers: 72.55.+s, 75.78.-n,75.50.Pp,62.65.+k,76.50.+g,68.60.-p

arXiv:1406.6483v1 [cond-mat.mtrl-sci] 25 Jun 2014

I. INTRODUCTION

Magnetostriction is the interaction between strain and magnetization, which leads to a change in a magnetic sample's shape when its magnetization is modified[1]. The opposite effect, inverse magnetostriction, whereby magnetization can be changed upon application of a strain, is particularly relevant to magnetic data storage technologies as a possible route towards induction-free data manipulation when used dynamically. It has been proposed for magnetization switching through resonant[2] or non-resonant processes[3,4]. Experimental results on magneto-acoustic coupling have been obtained in various configurations, either all optical[5] or all-electric[6–11]. The latter consists in the radio-frequency (rf) excitation of interdigitated transducers (IDTs) deposited onto a piezoelectric/ferromagnetic bilayer. This has for instance led to the extensive theoretical and experimental investigation of magnetization precession triggered by surface or bulk acoustic waves (resp. SAWs, BAWs) in Ni based films since the 1960s[6–8,10,12]. Elegant data has also been obtained more recently on Yttrium Iron Garnet, where BAWs were used to build a magnetic field tunable acoustic resonator[11].

No demonstration of SAW-induced ferromagnetic resonance has been shown in dilute magnetic semi-conductors (DMS). Yet these materials, such as (Ga,Mn)(As,P), are an interesting system since their magnetostrictive coefficients vary strongly with temperature. This provides an excellent tool to develop and validate theoretical models. Their low Curie temperature (100 - 180 K) imposes to generate SAWs at cryogenic temperatures, but their magnetization precession frequencies are close to accessible SAW frequencies (GHz) and their small and tunable magnetic anisotropy make them a good candidate for SAW-assisted magnetization switching[2].

In this paper, we evidence experimentally SAW-driven ferromagnetic resonance in a thin film of (Ga,Mn)(As,P) excited at 549 MHz, between 5 and 85 K (Sec. III). Both acoustic attenuation and velocity variations are monitored in the time-domain. We then solve the coupled magnetization and elastic dynamics equations and determine with a good match to the experimental data (Sec. IV) the expected resonance fields and acoustic resonance shape.

II. EXPERIMENTAL METHODS

A d=50 nm thick layer of $(Ga_{1-x},Mn_x)(As_{1-y},P_y)$ was grown by molecular beam epitaxy. After a 1h/250°C anneal, its Curie temperature reached T_c = 105 K and its active Mn concentration $x^{eff} \approx 3.5\%$. Since GaAs is only weakly piezoelectric, a 70/250 nm bilayer of SiO_2/ZnO was sputtered onto the magnetic layer. The silica underlayer was required for good adhesion. Care was taken to keep the substrate holder at relatively low temperature (150°C) during the ZnO deposition so as to not further anneal the magnetic layer. The Phosphorus ($y \approx 4\%$) was necessary to induce tensile strain in the layer, in order to obtain a dominantly uniaxial magnetic anisotropy[13,14], spontaneously aligning the magnetiza-

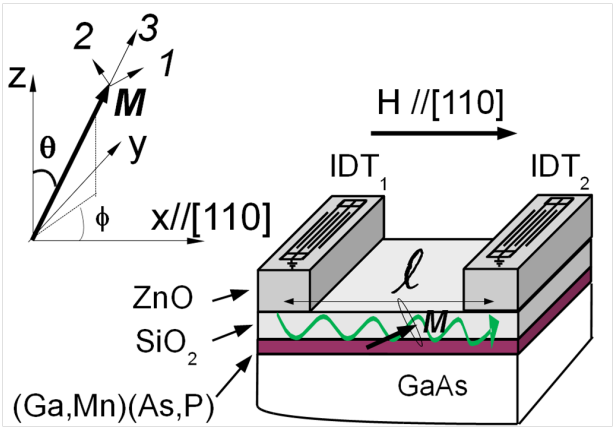

FIG. 1. Structure of the sample (not to scale). 50 nm ferromagnetic epilayer, 70 nm SiO_2 buffer, 250 nm piezoelectric ZnO. The IDTs are separated by 2 mm, but the effective length of the delay line is taken center-to-center of the IDTs, i.e l=2.3 mm. (upper left) Definition of the (x,y,z) and (1,2,3) reference frames.

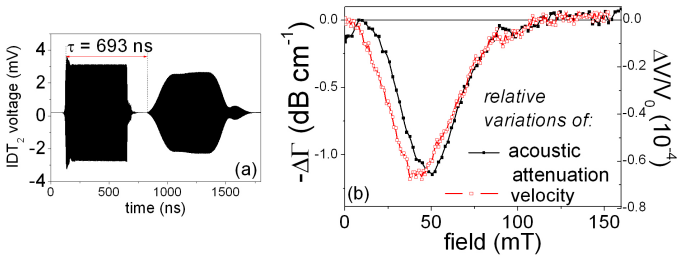

FIG. 2. (a) Receiving IDT signal: the electromagnetic field radiated by the emitter is shortly followed by the transmitted surface acoustic wave. T=120K, 549 MHz. (b) Attenuation changes and relative velocity variations at T = 80K. The opposite of $\Delta\Gamma$ has been plotted in order to highlight the different resonant field from the velocity variations.

tion perpendicular-to-plane. The resulting lattice mismatch of the layer to the substrate was of -1610 ppm.

Cr/Au interdigitated transducers (sixty pairs, thickness 10/80 nm) were then evaporated and a window opened in the ZnO layer between the two IDTs (Fig. 1). The metallization ratio of 0.5 and teeth width of 1.25 μm, yielded an acoustic wavelength of 5 μm. The emitter (IDT_1) was excited by 550 ns bursts of rf voltage modulated at 1 kHz. After propagation along the [110] direction, the SAW was detected by the receiver IDT_2 and the signal was acquired with a digital oscilloscope over typically 4000 averages. This time-domain technique allowed us to (i) verify that the SAWs were indeed generated/detected in the sample, and (ii) clearly separate the antenna-like radiation of IDT_1 (traveling at the speed of light), from the acoustic echo (traveling at the Rayleigh velocity), as shown in Fig. 2a. The transit time lies around τ=693 ns, which immediately gives an experimental estimation of the Rayleigh velocity $V_r \approx 2886$ m s^{-1}. The transfer function of the device exhibited the typical band-pass behavior centered at the 549 MHz resonance frequency (FWHM of 8 MHz). The power applied to the IDT_1 was of +20dBm (100 mW) on a 50 ohm load. The excitation frequency was $\omega/2\pi$=549 MHz.

The field/temperature-dependent measurements were done in a cryostat allowing rf cables to be brought down to the sample, which could be cooled down to 2.7 K. Unless specified, the field was applied in the plane of the sample, along the SAW wave-vector, i.e along a hard magnetic axis, and swept at 0.23 mT s^{-1}. A phase detection scheme then yielded the amplitude A and the phase $\phi = \omega\tau$ of the transmitted SAW. The phase variations $\Delta\phi$ were converted into relative velocity variations using $\Delta V/V_0 = \frac{\Delta\phi}{\omega\tau_0}$. The attenuation changes were computed using $\Delta\Gamma = -\frac{20}{l}\log\frac{A}{A_0}$. A_0 is an arbitrary reference amplitude. $l = 2.3mm$ and $\tau_0 = 797$ns are the IDTs ' center-to-center distance and the corresponding transit time.

III. EXPERIMENTAL RESULTS

A typical sweep at T = 80K is shown in Fig. 2b. Acoustic attenuation and velocity variations were both identical at low and high fields, but showed a clear feature at a particular field, hereafter called resonance field. The resonance disappeared above 90 K. Measurements down to 5 K showed that the amplitude of the effect steadily increased with decreasing temperature (Fig. 3). The resonance field was however not monotonous with temperature, lying within 35-94 mT with a maximum at 30-40 K. The resonance width followed the same trend, within the bounds 9-17 mT (error bars in Fig. 4b). All curves shared the following features: a fairly symmetrical, non-hysteretic resonance, with the velocity variations systematically resonating at a lower field than the amplitude variations. The maximum variation of acoustic attenuation, $\Delta\Gamma$= 8.5 dB cm^{-1} was observed at T=5 K. It remains weak compared to the value of 200 dB cm^{-1} measured at 2.24 GHz on a similar device on Nickel[9]. This is due to both the higher SAW frequency used by these authors, as the amplitude variations are directly proportional to ω (see Eqs. (24,27) of Ref. 10 for instance), and the much lower magneto-strictive constants found in DMS. These are defined as the fractional change in sample length as the magnetization increases from zero to its saturation value and their maximum values lie around $|\lambda_{100}| \approx$ 9 ppm for (Ga,Mn)As[15] and $\lambda_{100} \approx$50 ppm for Nickel[1]. Finally, we can easily check that the resonance frequency of the transducers is only very weakly modified by the magneto-elastic interaction: since $|\Delta\phi/\phi_0|=|\Delta\omega/\omega|\approx 10^{-4}$, typical velocity variations measured at $\omega/2\pi$=549 MHz yield a frequency change of a negligible ≈55 kHz.

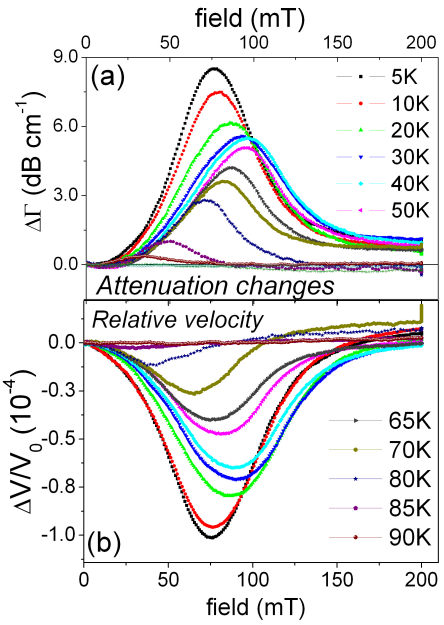

FIG. 3. (a) Variation of acoustic attenuation and (b) relative velocity change of the SAW between 5 K and 90 K.

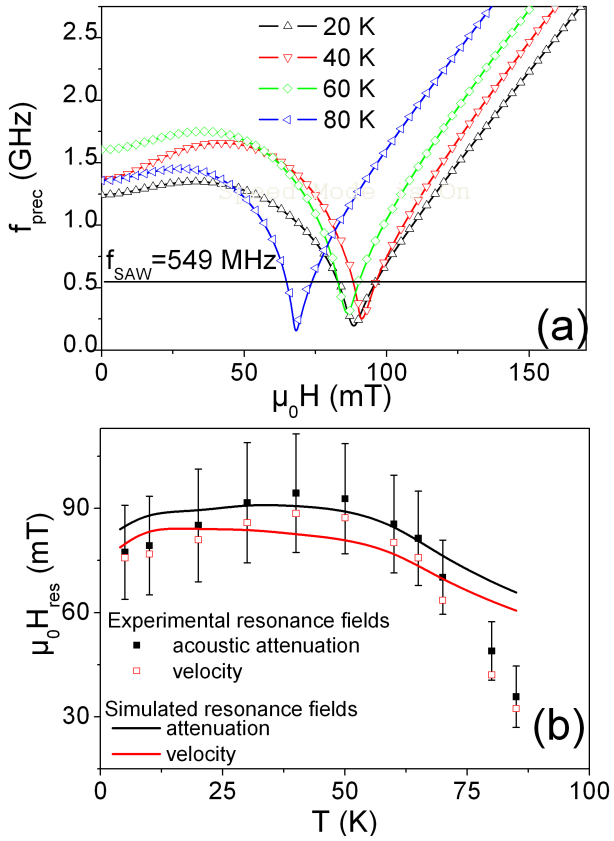

FIG. 4. (a) Calculated precession frequency versus field applied along [110], no sample tilt. The horizontal line indicates the SAW frequency. (b) Measured (symbols) and simulated resonance fields (dashed line, sample tilt 1.2°, taking into account both $A_{2\varepsilon}$ and $A_{4\varepsilon}$) versus temperature for the attenuation (black) and velocity (red) variations. The error bars correspond to the full width at half maximum of the resonance.

IV. MODEL

We have shown above that at a particular applied field, the transmitted SAW was slightly absorbed (by a 19% decrease in amplitude at 5 K), and delayed (by about...90 ps !) through its interaction with the magnetization of the (Ga,Mn)(As,P) layer. To confirm that this is indeed SAW-driven ferromagnetic resonance, we calculate the expected resonance fields and shapes. Microscopically, the resonance may be seen as the crossing of magnon and phonon dispersion curves at the wave-vector imposed by the IDTs, k_{SAW}. Macroscopically, the total energy of the system may then be written[16] :

$$E_{tot} = W + M_s F_{mc} + M_s F_{ms} \tag{1}$$

With:

$$W = \frac{1}{2} c_{ijkl}\varepsilon_{ij}\varepsilon_{kl} = W_0 + W_{SAW}(t) \tag{2}$$

$$F_{ms} = F_{ms,0} + F_{ms,SAW} \tag{3}$$

$$= (\varepsilon_{zz} - \frac{\varepsilon_{xx}+\varepsilon_{yy}}{2})[(A_{2\varepsilon}+A_{4\varepsilon})m_z^2 \tag{4}$$

$$+ \frac{A_{4\varepsilon}}{2} m_z^4 + A_{4\varepsilon}(m_x^4 + m_y^4)]$$

$$F_{mc} = -\mu_0 \vec{H}.\vec{m} + [\frac{\mu_0 M_s}{2} - 3B_c]m_z^2 + \frac{5}{2}B_c m_z^4 \tag{5}$$

$$- B_c(m_x^4 + m_y^4) + \frac{B_{2||}}{4}(m_x^2 - m_y^2)$$

The components of the unit magnetization vector are defined as m_i=M_i/M_s (i=x,y,z) where M_s is the magnetization at saturation and x//[110]. W is the purely elastic contribution and F_{mc} is the purely magnetic energy (magneto-crystalline, demagnetizing and Zeeman contributions, in units of field). In the latter, H is the applied field, B_c the cubic anisotropy constant and $B_{2||}$ the uniaxial one, distinguishing in-plane [110] and [1-10] axes[17]. F_{ms} is the magneto-elastic contribution (in units of field) where the magnetostrictive coefficients $A_{2\varepsilon}$, $A_{4\varepsilon}$ depend on both the static strain felt by the layer ($\varepsilon_{xx,0}, \varepsilon_{yy,0}, \varepsilon_{zz,0}$), and the dynamic SAW-induced strain ($\varepsilon_{xx,SAW}(t)$, $\varepsilon_{zz,SAW}(t)$). The $\varepsilon_{xz,SAW}(t)$ component of the SAW does not have any magnetostrictive action on the layer, and $\varepsilon_{yy,SAW}(t)$ is not excited by our set-up. The total strain components are thus given by $\varepsilon_{ii} = \varepsilon_{ii,0} + \varepsilon_{ii,SAW}(t)$. The magnetization and acoustics dynamics are then obtained by solving the Landau-Lifshitz Gilbert equation (LLG, Eq. 6) and the elastic wave equation (EWE, Eq. 7):

$$\frac{\partial \vec{m}}{\partial t} = \frac{\gamma}{M_s}\vec{m} \times \vec{\nabla}_{\vec{m}} E_{tot} + \alpha \vec{m} \times \frac{\partial \vec{m}}{\partial t} \quad (6)$$

$$\rho \frac{\partial^2 R_{tot,i}}{\partial t^2} = \frac{\partial \sigma_{ik}}{\partial x_k} = \frac{\partial}{\partial x_k}\frac{\partial E_{tot}}{\partial \varepsilon_{ik}} \quad (7)$$

where α is an effective damping constant and γ the gyromagnetic factor. $\vec{m}$=$\vec{m_0}$ + $\vec{m}(t)$ is the sum of the equilibrium magnetization unit vector and the rf magnetization and likewise for the displacement $\vec{R}_{tot}$=$\vec{R}_0$+$\vec{u}(t)$. The displacements are related to the strain by $\varepsilon_{ij} = \frac{\partial R_{tot,i}}{\partial x_j}$, ρ is the material density and c_{ijkl} the elastic constant tensor defined in the x,y,z frame (see Appendix B). Note that, as assumed by other authors[10,12] the exchange contribution was neglected in Eq. (6), as the typical SAW wave-vector ($\approx 1/\Lambda_{SAW}$) is much smaller than the first spin-wave wave-vector ($\approx 1/d$), leading to an essentially flat magnon dispersion curve for the frequencies considered here. For this reason, although we should in all rigor be talking about "spin-wave FMR", we will use the shorter term "ferromagnetic resonance".

Following Dreher et al.[10], we define a second reference frame (1,2,3) where $\vec{m_3}$ is aligned with the static magnetization (polar coordinates (θ_0, ϕ_0), see Appendix A). We are then left with two sets of unknowns: $(m_1, m_2)(t)$ (magnetization dynamics) and (u_x, u_z)(t) (acoustic dynamics), as the transverse displacement u_y cannot be excited by our device. Solving Eq. (6) in the linear approximation with $m_i(x,t)$=$m_{0,i}e^{i(\Omega t - kx)}$ leads to the following system:

$$\begin{pmatrix} m_1 \\ m_2 \end{pmatrix} = [\chi] \begin{pmatrix} \mu_0 h_1 \\ \mu_0 h_2 \end{pmatrix} \quad (8)$$

The dynamic fields are defined by $\mu_0 h_i = -\frac{\partial F_{ms,SAW}}{\partial m_i} \mid_{\vec{m}=\vec{m}_3}$. Since the uniaxial term $A_{2\varepsilon}$ ($\approx$ 40-60T) is around 10 times larger than $A_{4\varepsilon}$, the $A_{4\varepsilon}$ terms will be neglected. The dynamic magneto-elastic energy then simply reads: $F_{ms,SAW} = A_{2\varepsilon}\Delta\varepsilon(t)m_z^2$, so that $\mu_0 h_1$=$A_{2\varepsilon}\Delta\varepsilon(t)(cos^2\theta_0 - sin2\theta_0 m_1)$ and $\mu_0 h_2$=0.

The susceptibility tensor $[\chi]$ (given in Appendix A) depends on the static magnetic anisotropy constants, the damping and the SAW excitation frequency ω. Canceling the determinant of $[\chi]^{-1}$ yields the precession frequency (real part of Ω) $\left(\frac{\omega_{prec}}{\gamma}\right)^2 = (F_{11} - F_{33})(F_{22} - F_{33}) - F_{12}^2$ where the terms F_{ij} stand for $\frac{\partial^2(F_{mc}+F_{ms,0})}{\partial m_i \partial m_j}$. Fig. 4a shows the field-dependence of this precession frequency at various temperatures, calculated from the FMR anisotropy coefficients. $f_{prec}(\mu_0 H)$ first decreases, crossing the SAW frequency of 549 MHz (full line in Fig. 4a) at a particular field. When the magnetization is aligned with the field (saturated), f_{prec} reaches a minimum. After saturation, the resonance frequency increases with field, and crosses f_{SAW} a second time. We will show below that this second crossing does not give rise to any magneto-acoustic resonance. The crossover fields of $f_{prec}(\mu_0 H)$ with f_{SAW} (Fig. 4a) can already give a good approximation of the expected resonance fields. It is however not sufficient to explain why the resonance fields are different for relative variations of the SAW attenuation and velocity. For this it is necessary to calculate how the SAW wave-vector is modified by its interaction with the (Ga,Mn)(As,P) layer.

We place ourselves in the semi-infinite medium approximation and assume the SiO_2 layer to be a small perturbation to the system since its thickness is much smaller than Λ_{SAW} (see Appendix C for details on this point). With a general form of displacement, $u_i(x,t)$=$U_i e^{-\beta z} exp[i(\omega t - kx)]$ and using the equilibrium conditions on the strain, the EWE may then be simplified into:

$$\left(\rho\omega^2 + (\frac{A_\chi}{4} - c_{11})k^2 + c_{44}\beta^2\right) u_x + (c_{44} + c_{13} + \frac{A_\chi}{2})\beta i k u_z = 0 \quad (9)$$

$$(c_{44} + c_{13} + \frac{A_\chi}{2})\beta i k u_x + \left(\rho\omega^2 + (c_{33} - A_\chi)\beta^2 - k^2 c_{44}\right) u_z = 0 \quad (10)$$

Here we have introduced the complex constant:

$$A_\chi = M_s A_{2\varepsilon}^2 sin^2(2\theta_0)\chi_{11} \quad (11)$$

Two features come out. Firstly, this system is the formal equivalent of the solution to the EWE in a cubic, non-magnetostrictive material, with three of the elastic constants modified as follows:

$$\begin{aligned} c_{13} &\mapsto c'_{13} = c_{13} + A_\chi/2 \\ c_{11} &\mapsto c'_{11} = c_{11} - A_\chi/4 \\ c_{33} &\mapsto c'_{33} = c_{33} - A_\chi \end{aligned} \quad (12)$$

The elastic constants are modified through A_χ which depends on the applied field, the anisotropy constants and the SAW frequency (through χ_{11}). The real part of A_χ represents at most $\approx$10% of the GaAs elastic constants. This constant embodies the physics of the coupled magnon-phonon system as it modifies the elastic constants of the material. It cancels out when the material ceases to be magneto-strictive ($A_{2\varepsilon}$=0) and/or when the magnetization is colinear or normal to the SAW wave-vector. This is why no acoustic resonance is observed at the second crossing of $f_{prec}(\mu_0 H)$ with f_{SAW}, once the magnetization is aligned with the applied field ($A_\chi|_{\theta_0=\pi/2} = 0$). To check this point, we repeated the experiment with the field applied perpendicular to the sample this time : no resonance was observed, either in the attenuation changes or in the velocity variations.

Secondly, using the full depth-dependence of the displacements results in a coupling of the u_x and u_z components (β terms in Eqs. 9,10), contrary to simpler cases treated previously[10]. In fact, it is through the z attenuation that c_{13} and c_{33} constants are modified by the

magneto-strictive interaction; they would otherwise be left unchanged.

Canceling the determinant of Eqs. (9,10) yields two solutions with the corresponding absorption coefficients $\beta_{1,2}$ and x,z amplitude ratios U_z/U_x=r_i (i=1,2, see Appendix D). As neither of these satisfy the normal boundary condition $\sigma_{xz}|_{z=0} = 0$ at the vacuum interface, a linear combination of these two solutions needs to be considered:

$$u_x = [U_{x1}\exp(-\beta_1 z) + U_{x2}\exp(-\beta_2 z)]\, e^{i(\omega t - kx)} \quad (13)$$

$$u_z = [U_{z1}\exp(-\beta_1 z) + U_{z2}\exp(-\beta_2 z)]\, e^{i(\omega t - kx)} \quad (14)$$

The boundary conditions $\sigma_{xz}|_{z=0} = \sigma_{zz}|_{z=0}$=0 now lead to a new system, similar to Eqs. (9,10). Replacing r_i, β_i by their expressions and using ω/V_r=k, its determinant eventually leads to Eq. (15). This implicit polynomial equation in k may be solved numerically to yield the wave-vector solutions k_{sol} in presence of magneto-strictive interaction. There are three distinct physical solutions to Eq. (15), but only the Rayleigh surface wave can be excited by our device[18].

In the absence of magneto-striction, the usual Rayleigh velocity[19] $V_r = \frac{\omega}{k_{sol}|_{A_\chi=0}}$=2852.2 m s^{-1} is recovered, very close to the crude experimental estimation made earlier.

$$\left(c_{44} - \rho\frac{\omega^2}{k^2}\right)\left[c'_{11}c'_{33} - c'^2_{13} - c'_{33}\rho\frac{\omega^2}{k^2}\right]^2 = c'_{33}c_{44}\left(c'_{11} - \rho\frac{\omega^2}{k^2}\right)\left(\rho\frac{\omega^2}{k^2}\right)^2 \quad (15)$$

The amplitude of the transmitted SAW wave-vector is proportional to $\exp[-Im(k_{sol})l]$, and its phase is equal to $Re(k_{sol})l$. The relative variations are calculated with respect to the zero-field values. We can now plot the expected relative variations of acoustic attenuation and velocity (e.g. at 40 K, Fig. 5) assuming we excite the IDTs at 549 MHz. In this calculation, we have also taken into account the $A_{4\varepsilon}$ term. The procedure is identical to the one described above, but the expressions somewhat more cumbersome (see Appendix E for the corresponding effective elastic constants).

V. DISCUSSION

The relative variation of *attenuation* (Fig. 5, full black line) is monopolar and peaks at 88 mT, as expected from the simple crossing of $f_{prec}(\mu_0 H)$ with $f_{SAW} = \omega/2\pi$ (Fig. 4). The relative variation of *velocity* (full red line) is bipolar, and cancels out when the amplitude variation is maximum. Both curves are quite asymmetric, plummeting to zero when the magnetization is aligned with the field (92 mT). Introducing a small 1.2° sample tilt in the (x,z) plane with respect to the field direction pushes the saturation field away from the resonance field, restoring the symmetry of the resonance. This tilt may have been introduced when gluing the sample. It strongly reduces the magnitude of the effect, almost by a factor of 20. The attenuation resonance fields thus obtained are slightly higher than without tilt. The higher-field bump of the velocity variations disappears, making the resonance unipolar and at lower fields than the amplitude variations, as observed experimentally. It is interesting to compare these results to those of Dreher et al.[10], computed using a similar approach for an in-plane Nickel thin film. Their closest comparable configuration is the one where the field is applied close to the sample normal (hard axis configuration). Their simulations (last line of Fig. 8 in Ref. 10) also show that a bipolar shape is expected for the relative velocity, as the sample is excited closer and closer to its resonance frequency. Their experiments however also seem to show more of a monopolar behavior, for fields close to the sample normal.

Simulated attenuation and velocity variations resonance fields are now plotted along with the experimental ones in Fig. 4b as a function of temperature. Their values are well reproduced, so is their non-monotonous temperature variation. The latter can be traced back to a sign inversion of the $B_{2||}$ term with temperature i.e. a swap between [110] and [1-10] easy axes around 40 K.

Note that the magnetostrictive constants had to be reduced by a filling factor F to best reproduce the amplitude of the effect since the magnetic layer occupies a small portion of the volume swept by the SAW: $A_{2\varepsilon} \mapsto FA_{2\varepsilon}$, $A_{4\varepsilon} \mapsto FA_{4\varepsilon}$. This effective medium approximation is routinely used in other solid state physics systems, such as the case of sparse quantum dots embedded in a wave-guide[20]. A naive approach would lead us to expect $F \approx d/\Lambda_{SAW}$=0.01, whereas we converged to a value over ten times larger, $F = 0.10$ to obtain a good agreement between simulated and experimental attenuation variations. The simulated velocity variations are then however off by about an order of magnitude compared to the experiment (Fig. 5). We believe however that this filling factor has little physical meaning. Firstly, we have shown that not only F, but also the sample tilt play a great role in the amplitude of the effect, and this value is not known experimentally. Secondly, the SAW amplitude is in fact not uniform across the depth Λ_{SAW}: it decreases rapidly away from the surface (see for instance Fig. 1b of Ref. 2), so that the relative "weight" of the first d=50 nm is larger than d/Λ_{SAW}. To best

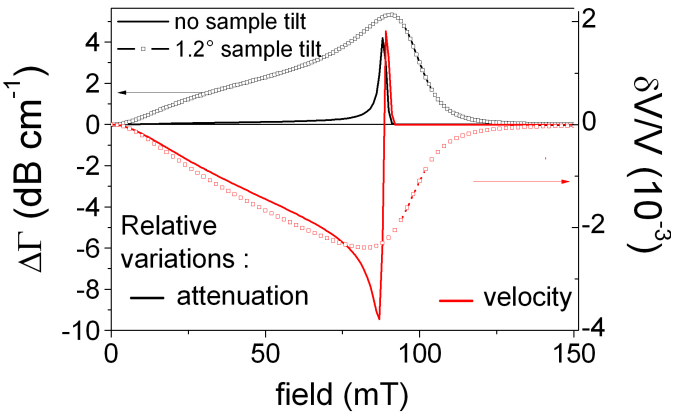

FIG. 5. Relative variations of the acoustic attenuation (black) and velocity (red) calculated with the T=40 K micromagnetic parameters, α=0.1 and F=0.105. The simulations were done taking into account both the $A_{2\varepsilon}$ and $A_{4\varepsilon}$ contributions, with (or without) a sample tilt in the (x,z) plane - symbols (full lines). The relative changes of attenuation and velocity without sample tilt have been divided by 20 for better visibility.

reproduce quantitatively and qualitatively the shape and amplitude of the effect a more complete multi-layer approach using a transfer matrix formalism would clearly need to be adopted, as was for instance done in Ref. 12.

VI. CONCLUSION

We have demonstrated the resonant excitation of magnetization precession in (Ga,Mn)(As,P) by a surface acoustic wave. Temperature-dependent measurements have clearly shown that the magnitude of the effect and the position of the resonance fields evolved with the magneto-strictive coefficient $A_{2\varepsilon}$. An analytical description of a SAW traveling through a magnetostrictive cubic medium was derived, and the SAW dynamics was found to be given by elastic tensor coefficients modified by a complex value proportional to $A^2_{2\varepsilon}$. This approach provides a very accurate way of predicting the resonance fields of SAW-driven FMR, an indispensable step towards SAW-induced precessional magnetization switching.

This work was performed in the framework of the MANGAS and the SPINSAW projects (ANR 2010-BLANC-0424-02, ANR 13-JS04-0001-01). We thank A. Lemaître (Laboratoire de Photonique et Nanostructures) for providing the (Ga,Mn)(As,P) sample, and M. Bernard (INSP) for helping us with the cryogenic set-up.

APPENDIX

A. Magnetization dynamics

Following Dreher et al.[10], the (1,2,3) reference frame is defined by $\vec{m}_3$ being aligned with the magnetization equilibrium position (θ_0,ϕ_0) and the following correspondence:

$$\begin{aligned} m_x &= m_1 cos\theta_0 cos\varphi_0 - m_2 sin\varphi_0 + m_3 sin\theta_0 cos\varphi_0 \\ m_y &= m_1 cos\theta_0 sin\varphi_0 + m_2 cos\varphi_0 + m_3 sin\theta_0 sin\varphi_0 \\ m_z &= -m_1 sin\theta_0 + m_3 cos\theta_0 \end{aligned} \tag{16}$$

The susceptibility tensor defined in Eq. (8) is given by:

$$[\chi] = \frac{1}{D}\begin{pmatrix} F_{22} - F_{33} + \frac{i\alpha\omega}{\gamma} & -(F_{12} - \frac{i\omega}{\gamma}) \\ -(F_{12} + \frac{i\omega}{\gamma}) & F_{11} - F_{33} + \frac{i\alpha\omega}{\gamma} \end{pmatrix} \tag{17}$$

where $F_{ij}=\frac{\partial^2(F_{mc}+F_{ms,0})}{\partial m_i \partial m_j}$ and

$$D = (F_{11} - F_{33} + \frac{i\alpha\omega}{\gamma})(F_{22} - F_{33} + \frac{i\alpha\omega}{\gamma}) - F_{12}^2 - \left(\frac{\omega}{\gamma}\right)^2$$

B. Elastic coefficient tensor

The elastic coefficient tensor being defined in the reference frame of a cubic material, we must rotate it by $\pi/4$ for the particular case of a SAW traveling along [110]. The equivalence with the usual elastic constants[19] C^0_{ij} is:

$$\begin{cases} c_{11} = \frac{1}{2}C^0_{11} + \frac{1}{2}C^0_{12} + C^0_{44} \\ c_{12} = \frac{1}{2}C^0_{11} + \frac{1}{2}C^0_{12} - C^0_{44} \\ c_{13} = C^0_{12} \\ c_{33} = C^0_{11} \\ c_{44} = C^0_{44} \\ c_{66} = \frac{1}{2}C^0_{11} - \frac{1}{2}C^0_{12} \end{cases} \tag{18}$$

Temperature variations of the elastic tensor have been neglected and (Ga,Mn)(As,P) elastic constants were assumed equal to those of GaAs.

C. Influence of the SiO_2/ZnO on the (Ga,Mn)(As,P) static strain

An important question is whether the high temperature (150°C) deposition of the SiO_2/ZnO bilayer modifies the magnetic layer's static strain. To check this,

we performed room temperature high resolution x-ray rocking curves around the (004) reflection at different steps of the bilayer deposition. The lattice mismatch of the reference (unpatterned) (Ga,Mn)(As,P) layer was around -1520 ppm, i.e under tensile strain on GaAs. After the SiO_2 deposition, the lattice mismatch dropped to -1360 ppm. However, the lattice mismatch of the layer after deposition of the full SiO_2/ZnO stack returned close to the reference value, around -1610 ppm, and remained unchanged after removal of the ZnO layer. The rocking curves also pointed to the presence of a strain gradient extending into the GaAs substrate subsequently to the SiO_2/ZnO deposition. Given that the static strain of the magnetic layer seems to be affected by SiO_2/ZnO deposition, the FMR measurements of the magnetic anisotropy constants were done on the (Ga,Mn)(As,P)/SiO_2/ZnO stack after removal of the ZnO.

D. Elastic wave equation

This paragraph details solutions to the elastic wave equation when taking the displacement as $u_i{=}U_i e^{-\beta z} exp[i(\omega t - kx)]$. Inserting this expression into Eq. (7) leads to the system of Eqs. (9,10). Canceling this determinant leads to the following bisquared equation in $q{=}\beta/k$ using the effective elastic tensor coefficients defined in Eq. 12:

$$q^4 + \frac{\left(-c_{44}^2 - c'_{11}c'_{33} + \left(c'_{13}+c_{44}\right)^2\right) + \rho V_r^2\left(c'_{33}+c_{44}\right)}{c'_{33}c_{44}} q^2 + \frac{\left(c'_{11}-\rho V_r^2\right)\left(c_{44}-\rho V_r^2\right)}{c'_{33}c_{44}} = 0 \tag{19}$$

This equation has two physical solutions, $q_i{=}\beta_i/k$ with $U_z/U_x = r_i$ (i=1,2) that verify:

$$q_1^2 + q_2^2 = \frac{\left(c_{44}^2 + c'_{11}c'_{33} - \left(c'_{13}+c_{44}\right)^2\right) - \rho V_r^2\left(c'_{33}+c_{44}\right)}{c'_{33}c_{44}} \tag{20}$$

$$q_1^2 q_2^2 = \frac{\left(c'_{11}-\rho V_r^2\right)\left(c_{44}-\rho V_r^2\right)}{c'_{33}c_{44}} \tag{21}$$

$$r_i = \frac{i\beta_i k\left(c'_{13}+c_{44}\right)}{k^2 c_{44} - \beta_i^2 c'_{33} - \rho\omega^2} (i=1,2) \tag{22}$$

As neither of these satisfy the normal boundary condition $\sigma_{xz}|_{z=0} = 0$ at the vacuum interface, a linear combinations of these two solutions needs to be considered, as further developed in the text.

E. Solutions when taking into account the $A_{4\varepsilon}$ term

At high temperatures ($T \geq T_c/2$), $A_{4\varepsilon}$ (cubic anisotropy) is routinely 10 smaller than $A_{2\varepsilon}$ (uniaxial anisotropy). At lower temperatures, we rather have $A_{2\varepsilon} \approx$ 4-5 $A_{2\varepsilon}$. Following the same calculation as in the text but taking into account $A_{4\varepsilon}$ gives the following modified elastic constants:

$$\begin{array}{c} c_{13} \mapsto c'_{13} = c_{13} + A_\xi DB \\ c_{11} \mapsto c'_{11} = c_{11} - A_\xi D^2 \\ c_{33} \mapsto c'_{33} = c_{33} - A_\xi B^2 \end{array} \tag{23}$$

where the magnetization is aligned by the field along a [±110] axis and

$$\begin{array}{c} A_\xi = M_s sin^2(2\theta_0)\chi_{11} \\ B = A_{2\varepsilon} + \frac{A_{4\varepsilon}}{2}(1 + 3cos(2\theta_0)) \\ D = B/2 \end{array} \tag{24}$$

The shape and position of the resonance remain globally unchanged, but the amplitude of the effect (on both the relative attenuation and the velocity variations) is strongly diminished.

[1] E. du Tremolet de la Lacheisserie, *Magnetism: Fundamentals*, Springer, 1st edition, 2006.

[2] L. Thevenard, J.-Y. Duquesne, E. Peronne, H. J. von Bardeleben, H. Jaffres, S. Ruttala, J.-M. George, A. Lemaître, and C. Gourdon, *Physical Review B* **87**, 144402 (2013).

[3] W. Li, P. Dhagat, and A. Jander, *IEEE Transactions on Magnetics* **48**, 4100 (2012).

[4] S. Davis, A. Baruth, and S. Adenwalla, *Applied Physics Letters* **97**, 232507 (2010).

[5] A. Scherbakov, A. Salasyuk, A. Akimov, X. Liu, M. Bombeck, C. Brüggemann, D. Yakovlev, V. Sapega, J. Furdyna, and M. Bayer, *Physical Review Letters* **105**, 117204 (2010).

[6] M. Pomerantz, *Physical Review Letters* **7**, 312 (1961).
[7] H. Bömmel and K. Dransfeld, *Phys. Rev. Lett.* **3**, 83 (1959).
[8] I.-a. Feng, *Journal of Applied Physics* **53**, 177 (1982).
[9] M. Weiler, L. Dreher, C. Heeg, H. Huebl, R. Gross, M. Brandt, and S. T. B. Goennenwein, *Physical Review Letters* **106**, 117601 (2011).
[10] L. Dreher, M. Weiler, M. Pernpeintner, H. Huebl, R. Gross, M. Brandt, and S. T. B. Goennenwein, *Physical Review B* **86**, 134415 (2012).
[11] N. Polzikova, a. O. Raevskii, and a. S. Goremykina, *Journal of Communications Technology and Electronics* **58**, 87 (2013).
[12] A. K. Ganguly, *Journal of Applied Physics* **47**, 2696 (1976).
[13] A. Lemaître, A. Miard, L. Travers, O. Mauguin, L. Largeau, C. Gourdon, V. Jeudy, M. Tran, and J. George, *Appl. Phys. Lett.* **93**, 21123 (2008).
[14] M. Cubukcu, H. J. von Bardeleben, K. Khazen, J. L. Cantin, O. Mauguin, L. Largeau, and A. Lemaître, *Physical Review B* **81**, 041202(R) (2010).
[15] S. C. Masmanidis, H. X. Tang, E. B. Myers, M. Li, K. D. Greve, G. Vermeulen, W. Van˜Roy, and M. Roukes, *Physical Review Letters* **95**, 187206 (2005).
[16] L. Landau, L. E. M, and L. Pitaevskii, *Electrodynamics of Continuous Media*, 1984.
[17] *This anisotropy has been attributed to the presence of a shear strain ϵ_{xy} in the [100] reference frame, which would imply that the SAW could have an action on it. However, since no experimental evidence of this shear strain has ever been shown, we have not taken it into account.*
[18] *There are two other physical solutions. Each of them is the superposition of bulk quasi-longitudinal and quasi-transverse acoustic waves traveling away from the surface. These components cannot be excited simultaneously by our device because Bragg's condition cannot be fulfilled simultaneously for both components.*
[19] R. I. Cottam and G. A. Saunders, *Journal of Physics C: Solid State Physics* **6**, 2105 (1973).
[20] R. Melet, V. Voliotis, A. Enderlin, D. Roditchev, X. Wang, T. Guillet, and R. Grousson, *Physical Review B* **78**, 073301 (2008).